Available online at www.sciencedirect.com

SCIENCE DIRECT®

Earth and Planetary Science Letters 227 (2004) 281–296

EPSL

www.elsevier.com/locate/epsl

Geochemical constraints on the regolith hypothesis for the middle Pleistocene transition

Martin Roy[a,b,*], Peter U. Clark[b], Grant M. Raisbeck[c], Françoise Yiou[c]

[a]*Lamont-Doherty Earth Observatory of Columbia University, 61 Route 9W, Palisades, NY 10964, USA*
[b]*Department of Geosciences, Oregon State University, Corvallis, OR 97331, USA*
[c]*Centre de Spectrométrie Nucléaire et de Spectrométrie de Masse, IN2P3-CNRS, Bât. 104 et 108, 91405, Orsay Campus, France*

Received 3 February 2004; received in revised form 9 August 2004; accepted 1 September 2004
Editor: E. Bard

Abstract

The transition from 41- to 100-kyr glacial cycles and concomitant increase in global ice volume ~1 Ma remain an enigmatic feature of late Cenozoic climate. Here, we examine the petrology, mineralogy, and geochemistry of the silicate fraction of tills spanning the past 2 Ma from the north-central United States to evaluate the hypothesis that this so-called middle Pleistocene transition (MPT) occurred by erosion of regolith and subsequent exposure of underlying Canadian Shield bedrock by the Laurentide ice sheet. These data indicate that late Pliocene tills are depleted in crystalline lithologies, unstable minerals, and major-element oxides derived from plagioclase and ferromagnesians and are enriched in kaolinite, quartz, iron oxides, TiO_2-bearing resistates, and meteoric ^{10}Be. In contrast, early and middle Pleistocene tills show enrichment in crystalline lithologies, stable minerals, and major oxides derived from plagioclase and ferromagnesians and depletion in meteoric ^{10}Be, whereas late Pleistocene tills show major-element concentrations that are most similar to that of fresh shield bedrock. Marine isotope records of Sr, Os, and Hf show significant changes around the MPT that are consistent with the removal of a regolith and the exhumation of fresh silicate bedrock. These results indicate that ice sheets initially expanded on highly weathered bedrock and progressively exhumed a fresher rock source, thereby supporting the hypothesis that a change in the composition of the substrate underlying ice sheets best explains the origin of the MPT.

Keywords: Laurentide ice sheet; Geochemistry; Paleoclimatology; glacial cycles; glacial sediments

1. Introduction

Continental ice sheets have repeatedly advanced and retreated across significant areas of the Northern Hemisphere since the onset of late Cenozoic glaciations at ~2.75 Ma. Deep-sea oxygen isotope ($\delta^{18}O$)

* Corresponding author. Tel.: +1 845 365 8603; fax: +1 845 365 8155.
E-mail address: mroy@ldeo.columbia.edu (M. Roy).

0012-821X/$ - see front matter © 2004 Elsevier B.V. All rights reserved.
doi:10.1016/j.epsl.2004.09.001

records measured on benthic foraminifera indicate that global ice volume varied at periodicities (23, 41, and 100 kyr) similar to the changes in the Earth's orbital parameters (precession, tilt, and eccentricity) during that time period [1–3]. High-resolution $\delta^{18}O$ records, however, show a transition in the middle Pleistocene (~1 Ma) from small ice-volume changes that varied largely at 41-kyr cycles to larger ice-volume changes that varied predominantly at 100-kyr cycles, despite the absence of any significant change in radiation forcing across that interval [3–6]. Similarly, eccentricity-driven insolation changes alone are too small to explain the large ice-volume response at the 100-kyr period [6].

A number of hypotheses have been proposed to explain this middle Pleistocene transition (MPT), but a consensus on its origin has yet to emerge [6,7]. Here, we address this issue by testing a hypothesis proposing that the MPT is related to a change in the character of the underlying geological substrate of the Laurentide ice sheet (LIS) and, possibly, other late Cenozoic ice sheets [8]. This hypothesis is based on marine records of $\delta^{18}O$ that indicate that global ice volume increased significantly after the MPT, while continental records indicate that ice sheets maintained a similar areal extent before and after the transition, thereby implying that the MPT also involved a change from thin to thick ice sheets (Fig. 1). Because studies of modern and former ice sheets indicate that ice sheet size and dynamics are strongly controlled by the geology of the subglacial substrate [9–11], these observations suggest that internal glaciological processes may have played a significant role in the origin of the MPT, as well as in the mechanisms that produced the 100-kyr cycle [8,11].

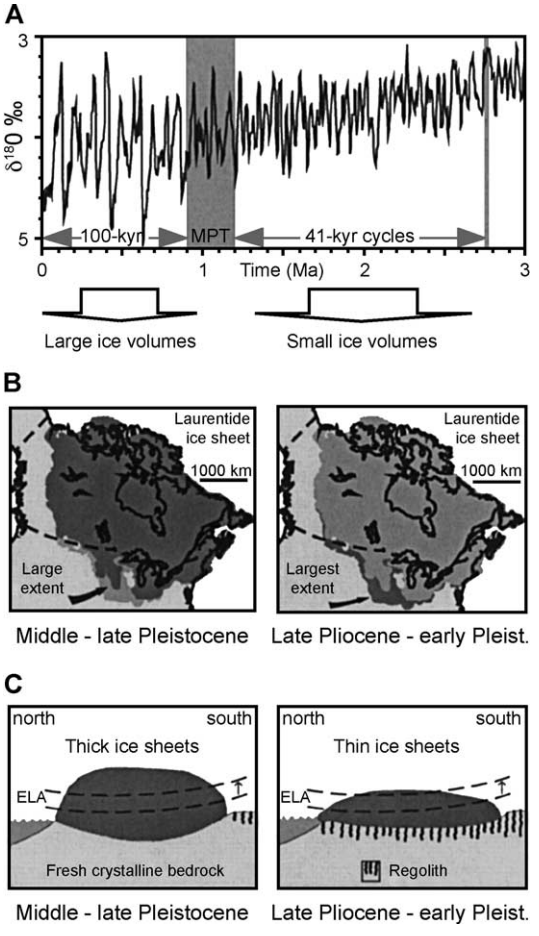

2. Strategy

Clark and Pollard [8] proposed that the MPT is a consequence of a change from ice sheets underlain entirely by soft beds to ice sheets underlain by a mixture of hard and soft beds. This change in the basal

Fig. 1. (A) Deep-sea oxygen isotope ($\delta^{18}O$) record of global ice volume variations for the last 3 Ma (ODP site 849, eastern equatorial Pacific [3]). The middle Pleistocene transition (MPT) is a change in the amplitude and frequency of glaciation cycles reflecting a shift from small to large volume ice sheets. (B) Areal extent of the Laurentide ice sheet. The maximum extent of the small volume (pre-MPT) ice sheets is similar or greater than that of the one of large volume (post-MPT) ice sheets. (C) Because the small- and large-volume ice sheets occupied the same surface area, the MPT also represents a change from thin to thick ice sheets. According to the hypothesis [8], ice sheets may have been resting on a regolith until ~1 Ma. Deformation of the water-saturated regolith by shear imposed by the overlying ice sheet resulted in thin, but areally extensive, ice sheets. The subsequent erosion of the regolith by the ice sheet uncovered the underlying fresh crystalline bedrock, providing a high-friction substrate that resulted in the development of larger, thicker ice sheets. The mass balance of an ice sheet depends primarily on the position of the equilibrium line of altitude (ELA), which moves in response to changes in solar radiation. Summer insolation maxima drive the ELA upwards, thereby causing a large fraction of the thin ice sheet to lie in a regime of net ablation, whereas a significant portion of the thick ice sheet remains in an accumulation regime. Accordingly, thin ice sheets would be more susceptible to deglaciation during insolation maxima, whereas some fraction of the thick ice sheets may survive into the next ice growth interval. This change in subglacial substrate may thus explain the onset of the 100-kyr glacial cycles.

boundary conditions of ice sheets occurred through the subglacial erosion of a thick regolith mantle that had formed through prolonged chemical weathering of crystalline bedrock prior to the initiation of Northern Hemisphere glaciation. Before the MPT, the regolith favored the development of thin ice sheets that responded linearly to the dominant 41-kyr orbital forcing. Successive glaciations eventually gave rise to the MPT through the subglacial erosion of the regolith and consequent unroofing of unweathered crystalline bedrock, thereby providing hard-bed conditions that induced a fundamental change in the response of ice sheets to orbital forcing (Fig. 1).

Our strategy in evaluating the regolith hypothesis is based on the fact that the bulk mineralogy and geochemistry of the regolith will be substantially distinct from that of the fresh parent bedrock [12–14]. Accordingly, tills derived from the erosion of the regolith should have a compositional signature that is different from that of tills derived from unweathered bedrock. Here, we document the composition of late Pliocene–Pleistocene glacial sediments of the north-central United States to evaluate whether till geochemistry, mineralogy, and petrology reflect a shift from the erosion of a regolith prior to the MPT to a fresh bedrock source afterwards.

3. Late Cenozoic glacial stratigraphy of the midcontinent

The midcontinent region (Fig. 2) is underlain by upper Pennsylvanian limestone, shale, and sandstone; most sections investigated here lie directly on carbonate bedrock. This region preserves extensive sedimentary sequences that record evidence of the late Pliocene and Pleistocene advances of the LIS [15]. The sequences consist of multiple tills interbedded with paleosols and nonglacial deposits, some of which contain volcanic ashes derived from eruptions of the Yellowstone caldera in Wyoming: Huckleberry Ridge ash (2.003 Ma), Mesa Falls ash (1.293 Ma), and Lava Creek ash (0.602 Ma) [16,17]. A till underlying an ash-bearing silt unit indicates that the oldest glacial deposit is more than 2 Ma [18]. The stratigraphic record identifies at least seven subsequent advances of the LIS across the region [19]. Advances of the LIS younger than ~250 ka have not reached the area [15].

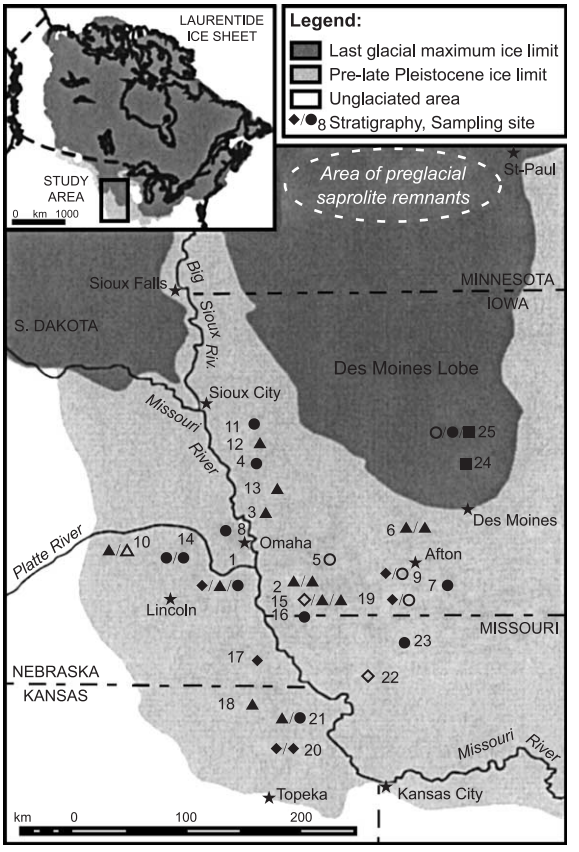

Fig. 2. Location of the stratigraphic sections investigated in relation to the maximum ice limit of late Cenozoic glaciations. Symbols correspond to the till stratigraphy exposed at each site (from bottom to top): ◆ are late Pliocene R2 tills (~2.7–1.3 Myr); are early Pleistocene R1 tills (~1.3–0.8 Myr); ● are middle Pleistocene N tills (~0.8–0.25 Myr); ■ are late Pleistocene LGM tills (~17 kyr). Age constraints are provided by three volcanic ashes and the Brunhes/Matuyama magnetic reversal [19]. Current chronological methods do not allow the dating of individual ice advances, and each till group represents multiple ice advances [19]. Open symbols correspond to till units with uncertain magnetic polarity but of lithological composition similar to their corresponding till-group category. Volcanic ash localities: sites 4, 8, 9, and 10. Site coordinates are given in Table 1.

Minimum age estimates from cosmogenic dating of striated bedrock outcrops in southwestern Minnesota indicate that these striations were formed ~575 ka [20], thereby suggesting that the region south of Minnesota was not affected, at least significantly, by subsequent ice advances during marine isotope stage (MIS) 6 (Illinoian). During the last glaciation, however, the Des Moines lobe advanced into the northern sector of the study area (Fig. 2).

Roy et al. [19] developed a chronological framework for the midcontinent glacial sequences based on the paleomagnetism of glacial and nonglacial deposits, and the stratigraphic relation of the three volcanic ashes to the till units. Paleomagnetic analyses distinguished tills deposited during the Brunhes Normal Chron from those deposited during the Matuyama Reverse Chron. Glacial deposits exhibit large variations in composition that, when placed in the context of the paleomagnetic and ash chronology, indicate significant lithological and mineralogical differences between tills of different age. From these relations, three pre-Illinoian till groups were distinguished ([19]; Fig. 2): an early Matuyama group (R2 tills), a late Matuyama group (R1 tills), and a middle Pleistocene Brunhes group (N tills). Tills deposited around the last glacial maximum (LGM) ~17 kyr represent a fourth group (LGM tills).

Midcontinent tills were consistently deposited by southward flowing glacial lobes (e.g., [21]), and the LIS configuration at the LGM indicates that these lobes were fed by a western flow line originating from the Keewatin ice dome [22]. A provenance study based on $^{40}Ar/^{39}Ar$ age determinations of K-feldspar and hornblende grains present within our sample indicates that this pattern of till deposition has prevailed for most of the last 2 Ma [23].

4. Methods

We obtained till samples from 25 stratigraphic sections (Fig. 2) exposed in rock quarries, roadcuts, and along riverbanks, and we drilled sediment cores at three localities where previous studies reported volcanic ashes interbedded with tills [24,25]. Within any given section, multiple glaciations are recorded by thick paleosols and/or nonglacial sorted sediments that generally separate 2–3 till units. Till unit thickness varies from 2 to 18 m, and sections commonly expose up to 30 m of glacial sediments, which are generally capped by extensive loess deposited during the last two glaciations. Midcontinent tills are typically fine grained, compact, and matrix dominated. These properties prevent groundwater migration and limit post-glacial weathering. All till samples were collected away from horizons affected by paleosol development or other post-depositional weathering features. Prior to sampling, sediment exposures were cleaned to a width of ~1 m and a depth of ~0.5 m, and fresh, unweathered material was collected for analyses. We also sampled LGM tills for comparisons between older tills and tills deposited under a fully developed 100-kyr cycle.

The <2 mm fraction of 28 till samples was leached of its carbonate content, and the major elements of the remaining silicate fraction were determined by X-ray fluorescence (XRF; Table 1). We also determined the mineralogy and petrology of these sediments [19]. The lithology of ~200 clasts (4–12.5 mm size fraction) of 95 samples was identified under microscope, and clast lithologies were grouped into sedimentary (carbonate, sandstone, and shale) and crystalline (igneous and metamorphic) lithologies. The mineralogy of the clay (<2 μm) and silt (<15 μm) fractions of 43 and 61 till samples, respectively, was analyzed using X-ray diffraction (XRD) techniques. The abundance of the main minerals in the XRD patterns was obtained through computer-assisted semiquantitative analyses [19].

5. Composition of the weathered and fresh rock source

Changes in the geological substrate that may be responsible for the MPT are presumed to have occurred in the so-called hard-bedded region associated with the igneous and metamorphic rocks of the Canadian Shield [8,11]. We thus use the average composition of the shield as the fresh rock end-member in the hypothesis. The composition of the Canadian Shield is comparable with that of the Average Upper Continental Crust (AUCC), which is, in turn, equivalent to that of a granodiorite [26–29]. Accordingly, we infer that the weathered end-member source originally developed on AUCC-type granodiorite. We are unable to further specify a specific source rock area due to uncertainties in the exact geometry of ice-flow trajectories and distance of glacial transport during the course of Northern Hemisphere glaciation. Tills, however, represent a mixture of different lithologies that were incorporated progressively during transport, thus, the silicate content of the midcontinent tills is likely to reflect a broad range of lithologies forming the Canadian Shield. Within this context, the

Table 1
Major-element oxide concentrations of tills[a], AUCC, and saprolite

Till group	Sample no.	Site no.	Latitude North	Longitude West	SiO_2 (wt.%)	Al_2O_3 (wt.%)	TiO_2 (wt.%)	FeO* (wt.%)	MnO (wt.%)	CaO (wt.%)	MgO (wt.%)	K_2O (wt.%)	Na_2O (wt.%)	P_2O_5 (wt.%)	LOI (%)
LGM	WHA01	24	42°01′45″	93°35′48″	78.14	9.50	0.370	2.34	0.0346	3.66	2.31	1.83	1.72	0.100	5.66
LGM	ALDO5	25	42°31′33″	93°22′15″	76.30	10.09	0.407	2.51	0.0370	4.16	2.75	1.93	1.69	0.117	7.09
N	ALD03	25	42°31′33″	93°22′15″	76.94	11.47	0.533	2.86	0.0191	2.65	1.98	1.97	1.48	0.091	6.57
N	CTY09	1	41°04′27″	95°57′50″	78.52	12.17	0.598	2.96	0.0141	0.80	1.13	2.15	1.60	0.064	5.80
N	FLO01	8	41°22′21″	95°56′51″	75.43	13.55	0.671	3.92	0.0272	1.49	1.43	2.23	1.07	0.183	6.66
N	FRE02	14	41°23′59″	96°31′24″	75.59	13.31	0.652	4.00	0.0443	1.41	1.50	2.29	1.04	0.173	7.39
N	FRE05	14	41°23′59″	96°31′24″	75.55	12.63	0.616	3.45	0.0483	2.18	1.96	2.24	1.18	0.132	6.93
N	LMR01	11	42°50′25″	96°08′56″	75.58	14.12	0.670	3.41	0.0171	1.27	1.40	2.27	1.11	0.152	5.80
N	MER03	23	40°30′31″	93°28′55″	76.41	13.04	0.648	3.38	0.0161	1.44	1.42	2.14	1.38	0.135	5.99
N	THA02	7	40°59′38″	94°02′25″	78.55	11.79	0.607	3.18	0.0182	1.46	1.35	1.96	0.97	0.120	4.93
N	STR01	16	40°45′05″	95°42′45″	80.08	10.28	0.509	2.62	0.0384	1.74	1.34	1.99	1.28	0.113	4.17
N	SHM04	4	41°51′20″	95°59′13″	75.85	13.35	0.664	3.94	0.0282	1.32	1.42	2.27	0.99	0.161	6.84
N	BEF04	19	40°40′24″	94°15′02″	76.61	13.38	0.712	4.03	0.0342	1.02	1.12	2.06	0.92	0.123	6.89
R1	CRSO2	3	41°20′59″	95°53′46″	76.19	11.72	0.682	3.97	0.0331	2.30	1.84	2.11	0.98	0.178	8.47
R1	DC141	10	41°14′59″	97°10′00″	75.43	12.61	0.629	4.11	0.0352	2.01	1.77	2.23	0.99	0.187	8.01
R1	GLW04	2	41°06′09″	95°49′20″	76.98	12.01	0.627	3.76	0.0313	1.78	1.64	2.05	0.95	0.171	7.00
R1	THU03	15	40°51′24″	95°45′30″	78.33	11.06	0.600	3.67	0.0285	1.74	1.46	2.00	0.96	0.169	6.33
R1	THU05	15	40°51′24″	95°45′30″	78.82	11.10	0.534	2.50	0.0192	2.00	1.61	2.07	1.24	0.104	5.77
R1	GRN02	6	41°27′32″	94°25′51″	76.79	11.73	0.630	3.69	0.0326	2.18	1.80	2.00	1.00	0.150	6.64
R1	TUR01	12	42°03′46″	95°59′13″	79.05	11.33	0.566	2.60	0.0161	1.50	1.26	2.14	1.45	0.095	4.95
R1	WAT01	21	39°44′34″	94°56′38″	76.33	12.09	0.634	3.98	0.0325	1.95	1.73	2.12	0.96	0.184	6.90
R2	AF172	9	40°59′46″	94°12′16″	78.63	11.68	0.737	3.91	0.0232	0.87	1.23	1.96	0.88	0.097	5.12
R2	ATC02	20	39°32′29″	95°10′09″	75.96	12.75	0.709	4.59	0.0331	1.12	1.38	2.33	0.96	0.178	5.49
R2	CTY04	1	41°04′27″	95°57′50″	81.96	10.08	0.584	2.36	0.0160	0.65	0.85	2.00	1.42	0.069	3.91
R2	ELC01	17	40°15′56″	96°09′37″	75.70	13.80	0.705	3.35	0.0231	0.70	1.50	2.56	1.57	0.079	6.25
R2	BEF02	19	40°40′24″	94°15′02″	78.12	12.27	0.749	3.55	0.0799	0.73	1.15	2.02	1.26	0.079	5.50
R2	SEN01	18	39°49′37″	96°03′09″	74.07	14.34	0.769	4.88	0.0323	1.04	1.45	2.45	0.79	0.178	6.82
R2	BET01	22	40°17′32″	94°00′13″	76.32	13.62	0.795	3.61	0.0220	0.57	1.31	2.26	1.39	0.103	5.26
n.a	AUCC[b]	n.a.	n.a.	n.a.	64.90	14.60	0.520	4.40	0.0700	4.10	2.20	3.10	3.50	0.150	n.a.
n.a	Sapro.[c]	n.a.	44°32′80″	95°04′90″	56.30	25.40	1.720	10.07	0.1600	0.42	1.18	4.50	0.16	0.090	n.a.

n.a.—Not applicable.

[a] Results obtained from XRF analysis; <2 mm size fraction of tills. The carbonate content of the sediment was leached using buffered acetic acid (pH 4.8); normalized results (wt.%), with total Fe expressed as FeO. See Fig. 2 for site location.

[b] AUCC—average upper continental crust [26]; here used as the general composition of the Canadian Shield.

[c] Sapro.—saprolite developed on granodiorite rock; data from site 31 of [14].

composition of the Shield is simply used to provide a common reference against which the composition of different-age tills can be compared.

The long-term effect of chemical weathering is to change the bulk mineralogy and geochemistry of the parent rock, resulting in the formation of a saprolite in which the compositional changes are greatest at the surface and progressively diminish with depth [12,13,30,31]. The overall composition of the weathering profile reflects the behavior of the original rock-forming minerals in response to weathering. In igneous rocks, plagioclase and amphibole are generally lost early to dissolution, followed by biotite, thereby leaving the upper saprolite rich in quartz, with some K-feldspars, along with minor amounts of muscovite and resistates (zircon, rutile, garnet, and ilmenite). The relative abundances of quartz, K-feldspars, and resistates are further enhanced in the upper saprolite by the loss of plagioclase and ferromagnesians [12]. The alteration of the major minerals gives rise to the formation of a wide range of secondary minerals (Al-rich clays and Fe-oxides). Intense and prolonged weathering conditions may also lead to desilication, with attendant transformation of kaolinite into gibbsite, and the production of goethite or hematite from Fe-bearing clays.

The mineral changes caused by weathering are accompanied by changes in elemental abundance. The alteration of plagioclase and ferromagnesians causes the release of the soluble elements Ca, Na, and Mg, which are mostly lost from the weathering profile. The greater resistance of K-feldspars is reflected by comparatively lesser loss of K. The behavior of Fe is complex, but the ferrous iron typically released from the crystalline rock is generally transformed into ferric hydroxide under oxidative weathering [31]. The release of elements with a lower solubility, i.e., primarily Si and Al from aluminosilicates, with minor amounts of Ti, Mn, Co, and Ni from ferromagnesians, are preserved in the profile, mainly as part of secondary minerals forming the weathering products [31,32].

Remnants of the regolith inferred in the MPT hypothesis occur in Minnesota, immediately north of the study area (Figs. 2 and 3), where a saprolite developed in Precambrian bedrock is preserved under glacial deposits of varying age [14,33]. Paleogeographic considerations suggest that this weathering profile is pre-Cretaceous in age and that it began developing in the late Jurassic, when Minnesota was located at subtropical or tropical latitudes [33]. This saprolite typically shows thicknesses of 45–60 m, exceeding 90 m in some places [14]. The upper saprolite consists of abundant kaolinite and other clays, whereas the lower facies display a gradual decrease in weathering products and concomitant increase in fresh parent rock materials (Fig. 3; [14,33]). Similar saprolite remnants have been found in several other locations formerly covered by the LIS, including Quebec and Labrador, the Appalachian Mountains, and the Maritimes of eastern Canada [34].

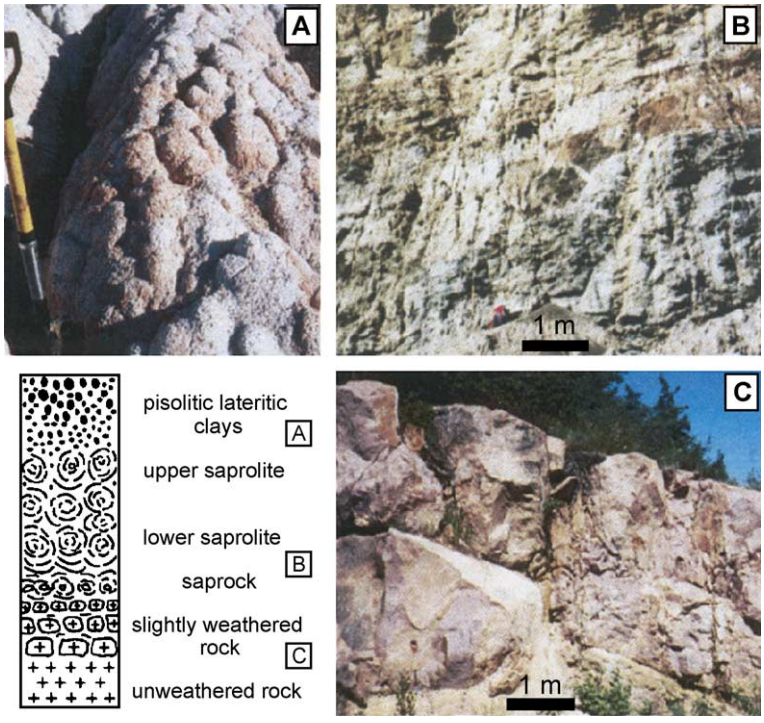

Fig. 3. Details of an extensive saprolite remnant preserved in the Minnesota River valley region (located in Fig. 2). The weathering profile (lower left) is typically 45–60 m in thickness and is divided into four facies according to the intensity of the weathering features, which decreases with depth [14]. Each facies is characterized by distinct Chemical Index of Alteration (CIA) values [14]: laterite with CIA values of 97–98; saprolite with CIA of 69–99; saprock with CIA of 56–71; and slightly weathered rock with CIA of 54–65. Fresh granite rock has CIA values of 47–53. (A) Pisolitic laterite clays. (B) Weathered granite rock still retaining the original structure fabric of the parent rock. (C) Weathering along joint fractures isolating blocks of fresh granite rock. CIA=$[Al_2O_3/(Al_2O_3+CaO^*+Na_2O+K_2O)]\times 100$, where CaO* is from silicate minerals [39].

Although the development of a regolith generally takes place over large areas and for long periods of time, the end result does not necessarily consist of a thick and homogenous regolith mantle. Spatial and depth variations in weathering products are typically present [14,32], and these irregularities within the regolith mantle must be accounted for when evaluating the provenance/source of regolith-derived sediments.

6. Till compositional results

6.1. Till lithology and mineralogy

A significant change in the composition in the midcontinent glacial deposits is recorded in the lithology of the clast fraction of tills, with an increase in the proportion of crystalline lithologies in progressively younger till sequences [19,25]. The late Pliocene R2 tills are depleted in crystalline lithologies (10–22%; 15% average), the early Pleistocene R1 tills have intermediate proportions (30–45%; average 37%), and the middle Pleistocene N tills and the LGM tills are enriched in crystalline lithologies (38–60%; average 47%; [19]).

The mineralogy of the clay and silt fractions also shows differences among the till groups. Although the clay fraction of all till groups is dominated by smectite, significant decreases in kaolinite and increases in chlorite occur in the N and LGM tills relative to the R2 and R1 tills [19]. The mineralogy of the silt fraction also shows significant contrasts among different-age tills. In particular, the N and LGM tills are characterized by increases in calcite, dolomite, and feldspars with respect to their quartz content, whereas the older reverse-polarity tills (R2 and R1 tills) are enriched in quartz [19].

Boellstorff [24] reported changes in the heavy mineral content of the fine-sand fraction of tills from the study area that also indicate systematic changes with time. Specifically, tills equivalent to R2 tills are enriched in weathered products (iron oxides and limonite) and depleted in unstable minerals (hornblende, biotite, and apatite), relative to the N tills. Furthermore, Gravenor [35] identified the presence of fragments of bauxite, a product of prolonged chemical weathering, in the R2-equivalent tills.

Finally, we note that additional mineralogical evidence for a change in source composition from weathered to unweathered material during the MPT comes from marine sediments from Baffin Bay (ODP core 645B), which record the erosion of the northeastern sector of the LIS. In particular, there is a marked decrease in kaolinite and expandable clays and an increase in illite, chlorite, and feldspars during the MPT [36,37].

6.2. Till geochemistry

The major-element chemistry of a saprolite developed on a granodiorite will be largely governed by the weathering of K-feldspars and Na- and Ca-rich plagioclases, which account for ~80% of the minerals susceptible to chemical weathering [13]. In addition to feldspar, the alteration of ferromagnesian minerals will also influence the distribution of major elements in the till groups, despite their much lower abundance in the rock source (~15%). Although some MgO can be partly retained in the saprolite as smectite, most of it is released from the profile [38]. In contrast, FeO is largely retained as secondary iron precipitates, such as goethite and hematite. Similarly, TiO_2 is highly immobile and is often adsorbed by newly formed minerals in the profile. TiO_2 is also found in resistate minerals such as rutile and ilmenite. Resistates may become concentrated in the upper profile due to the depletion of other mineral phases and may thus become reliable indicators of source composition [31,38]. For these reasons, we focus on geochemical indices that constrain the weathering of feldspars and ferromagnesians or reflect enrichment in resistate minerals.

We first compare the results of bulk geochemical analyses of the four till groups with the major-oxide concentrations of the Canadian Shield (i.e., AUCC-type granodiorite). In general, the averaged concentrations of major elements of tills are significantly different than the composition of fresh granodiorite (Fig. 4A). The main differences between the pre-Illinoian tills and the granodiorite are depletion in FeO, MnO, CaO, MgO, K_2O, and Na_2O and enrichment in SiO_2 and TiO_2. In contrast, the LGM tills are enriched in CaO, MnO, MgO, and Na_2O, depleted in TiO_2 and FeO, and are similar in SiO_2 and K_2O with respect to these older till groups. The N, R1, and R2

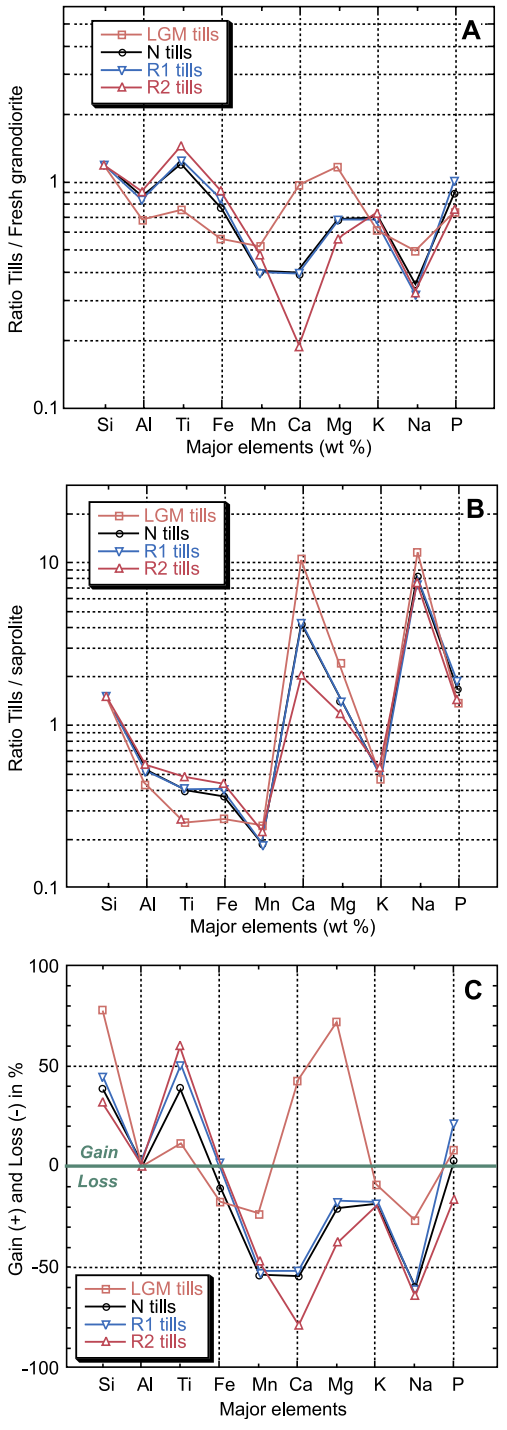

till groups show some variability among them, but there is a clear demarcation between these till groups and the LGM tills.

The LGM and R2 till groups exhibit the largest geochemical differences, whereas R1 and N tills have nearly identical compositions. When compared with a saprolite developed on a granodiorite [14], the R2 till group most closely resembles the upper part of the saprolite (Fig. 4B). The remaining till groups show concentrations that are more similar to the composition of the lower saprolite and unweathered rock, with LGM tills being most like fresh granodiorite.

We also report 'net' elemental gain and loss percentages for the till groups (Fig. 4C) to account for the 'closure effect' associated with chemical values expressed in weight percent ([38]; see Online Appendix) and to better distinguish the effect of weathering on the chemical composition of the rock source eroded by ice sheets. The depletion in labile elements (CaO, MgO, and Na_2O) in the older till groups relative to the younger till groups reflects the poor resistance of plagioclases and ferromagnesians to weathering and thus records initial erosion of a more weathered bedrock source. The differences in the K_2O content of the till groups are less pronounced, which may reflect the greater resistance of K-feldspars to weathering. The slight enrichment of FeO in R2 and R1 tills relative to N and LGM tills indicates that the older till groups derive from the erosion of a source enriched in secondary iron precipitates. Similarly, R2 tills are slightly enriched in TiO_2 compared with the R1 and N tills, whereas LGM tills are clearly depleted in TiO_2. The TiO_2 content of the older till groups indicates the erosion of a source rich in resistate minerals or reflects the low mobility of TiO_2 in the saprolite. The depletion of SiO_2 in R2 tills with respect to the R1 and N tills may also suggest the

Fig. 4. (A) Ratio diagram comparing the average composition of major-element oxides of the till groups to the bulk composition of the Canadian Shield [29], which corresponds to a AUCC-type granodiorite. (B) Ratio diagram comparing the average geochemical composition of each till group to the major elements of the upper part of a preglacial saprolite remnant developed on a granodiorite [14]. (C) Diagram showing net gain and loss percentages in the major oxides of till groups with respect to a fresh AUCC-type granodiorite (see Online Appendix for the calculation of net gain loss percentages). Number of samples analyzed in each till group: 2 LGM tills, 11 N tills, 8 R1 tills, and 7 R2 tills. The XRF data of the tills, AUCC, and saprolite are presented in Table 1.

erosion of the uppermost part of the weathering profile, where quartz was affected by pronounced leaching [14]. The marked increase in SiO_2 of LGM tills points towards a greater input of quartz, likely from the erosion of fresh crystalline rocks. Despite their depletion in SiO_2 concentrations relative to younger tills, R2 and R1 tills still show enrichment in SiO_2 compared with the AUCC, suggesting that quartz was a major constituent of the weathered profile.

We next evaluate differences in the geochemistry of the main till groups and their relation to source rock using ternary diagrams (Fig. 5). The Al–CaNa–K diagram mainly illustrates the weathering of feldspars and also depicts the Chemical Index of Alteration (CIA) that quantifies the degree of weathering to

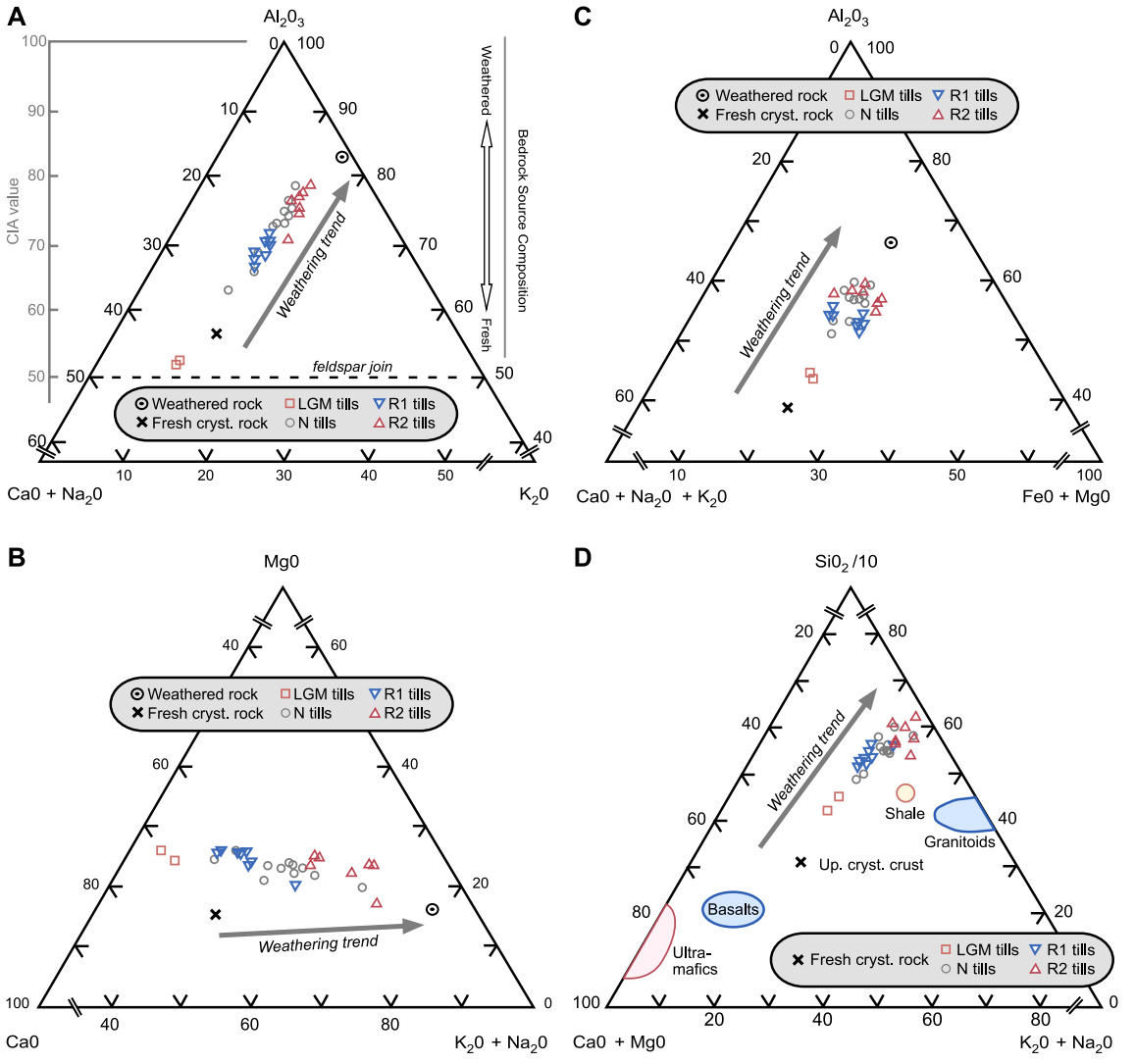

Fig. 5. Ternary diagrams showing the distribution of the geochemistry of samples from all till groups with respect to the weathering path of a fresh AUCC-type granodiorite source. (A) Diagram depicting the weathering of feldspars. CIA is the Chemical Index of Alteration [39]. CIA values of the R2, R1 and LGM tills correspond to the ones reported here for the saprolite, saprock, and fresh rock, respectively (see Fig. 3).(B) Weathering of feldspars vs. ferromagnesians. (C) Weathering of ferrogmagnesians vs. Ca-, Na-, and K-rich feldspars. (D) Composition of till groups vs. various rock sources. The weathered rock composition is the same as in Fig. 4.

which silicate minerals have been subjected prior to their erosion [39]. The values of the till groups fall parallel to a mixing line between fresh and weathered granodiorite rock end-members, the two rock sources inferred in the hypothesis (Fig. 5A). LGM tills plot close to the feldspar join, indicative of a fresh bedrock source. The values of R2 tills generally group in a cluster indicative of the erosion of a strongly weathered rock source. R1 tills cluster in a distribution that is between the LGM and the R2 tills, suggesting that R1 tills were derived from the erosion of a rock source slightly less weathered than the R2-till rock source, but not as fresh as the rock source of LGM tills. We find similar differences between the R2, R1, and LGM tills on the Mg–Ca–NaK and Al–CaNaK–FeMg diagrams (Fig. 5B and C), which show the effect of weathering on ferromagnesians with respect to Ca- and Na-plagioclase and K-feldspars. The Si/10–CaMg–NaK diagram (Fig. 5D) compares the geochemistry of all till groups to different rock sources.

In all cases, the distribution of N-till geochemical values overlaps the range spanned by the clusters of R2 and R1 tills. The geochemistry of N tills is, at first hand, surprising because it is opposite to their lithological and mineralogical contents, which suggest that N tills were derived primarily from the erosion of a fresh crystalline rock source, nearly similar in composition to that of LGM tills.

The results described above suggest that R2 tills were derived from the erosion of a highly weathered rock source, whereas R1 tills also derived from weathered rock, but from material that had originally been lower in the weathering profile and thus less enriched in weathered products. On the other hand, the geochemistry of LGM tills suggests a source from fresh crystalline bedrock. In this context, it is reasonable to expect that a source of unweathered rock should have been available for N tills. The geochemical signature of N tills may be complicated by the recycling of older deposits (R2 and R1 tills), which would provide a source of weathered material. We thus interpret the range in the distribution of N-till geochemical values to reflect recycling of preexisting tills and mixing with fresh, unweathered rock.

An additional factor that may have contributed to the differences between the lithology-mineralogy and the geochemistry of N tills is the fact that they were deposited during 100-kyr cycles. The chronology of the LIS during the last glaciation and inferences based on the structure of the $\delta^{18}O$ record suggest that the LIS ice margin remained near the outer boundary of the Canadian Shield for most of the last glacial cycle (i.e., the initial 80 kyr), only advancing to its maximum extent for a short period during MIS 2 [11,40]. Assuming that this pattern is representative of 100-kyr glaciations, in general, then extensive areas of bedrock and preexisting glacial sediments adjacent and distal to the Canadian Shield would have been exposed to long intervals of subaerial weathering during these extended nonglacial conditions. Studies of interglacial weathering rates from soil chronosequences developed in granitic moraines [41,42] suggest that 80-kyr-long interglacials result in weathering rates that are greater by four orders of magnitude than those of shorter interglacials, such as the ones associated with the 41-kyr cycles. The incorporation of this surficial weathered material by subsequent glaciations may thus have provided a source of material depleted in base cations to the N tills, thereby explaining their off-trend geochemistry.

6.3. Meteoric ^{10}Be in glacial sedimentary sequences

We further assess the regolith hypothesis by measuring meteoric ^{10}Be concentrations in till samples. Meteoric ^{10}Be refers to the ^{10}Be that is produced in the upper atmosphere. Precipitation removes this ^{10}Be, which is subsequently transferred to the Earth's surface by rainfall, and then efficiently trapped in soil by clay particles. Studies of soil chronosequences show that meteoric ^{10}Be abundance increases in soils of increasing age [43] and that an old saprolite can yield a large ^{10}Be inventory (i.e., 8.8×10^{11} atoms/cm^2; [44]). In the latter case, most of the high ^{10}Be concentrations ($\sim1.05\times10^9$ atoms/g) are found in the upper 1–5 m of the profile, where clays are abundant; below this horizon, ^{10}Be concentrations decrease exponentially with depth. These results demonstrate that the preglacial regolith mantle likely accumulated large amounts of ^{10}Be over time. Consequently, tills originating from the erosion of the upper part of this regolith should have higher ^{10}Be concentrations than will tills derived from the lower part of the regolith or fresh crystalline bedrock, in which ^{10}Be is virtually absent.

Table 2
Concentration of meteoric ^{10}Be in tills of different ages

Till group	Sample no.; site[a]	Sample age constraints (Ky)[b]			^{10}Be concentration (10^7 atom/g)[c]			
		Maximum	Minimum	Average	Measured	Corr. max.	Corr. min.	Corr. avg.
LGM	WHA1R; 24	17	17	17	5.62	5.67	5.67	5.67
N	FLO1R; 8	780	600	690	3.97	5.75	5.24	5.49
R1	CRS2R; 3	1300	780	1040	2.29	4.18	3.31	3.72
R1	DC139R; 10	1300	780	1040	3.69	6.73	5.34	5.99
R2	CTY3R; 1	2700	2000	2350	6.32	22.00	15.92	18.72
R2	AF172R; 9	2700	2000	2350	4.54	15.81	11.44	13.45

[a] Sample no.—sample number; see Fig. 2 for site location and Table 1 for site coordinates.
[b] Age constraints provided by three volcanic ashes (0.6, 1.3, and 2.0 Ma) and the Brunhes/Matuyama magnetic reversal (~0.78 Ma); see [19] for details.
[c] Corr.—concentration corrected for radioactive decay; max.—maximum age; min.—minimum age; avg.—average age.

We measured the ^{10}Be concentrations of six till samples with reasonably well-constrained ages (Table 2). We ground the <2 mm fraction of each till sample, added a calibrated spike of ^{9}Be carrier to ~1 g of sample, and then extracted the beryllium using a fusion method [45]. After oxidation of the samples to BeO, ^{10}Be/^{9}Be ratios were measured by accelerator mass spectrometry at the Gif-sur-Yvette Tandetron facility, relative to NIST standard (SRM 4325), using the certified ratio of 2.68×10^{-11}.

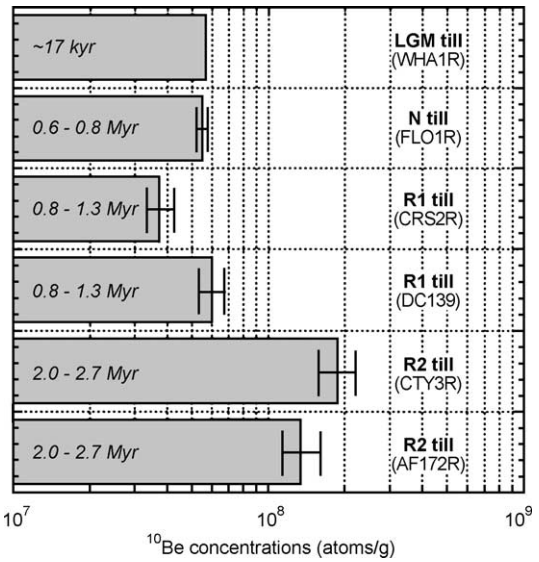

Fig. 6. A^{10}Be concentrations in tills of different ages, corrected for radioactive decay. The large horizontal bars represent mean concentrations with respect to the age constraints of each sample (Table 2). Thin vertical lines at the end of each horizontal bar represent concentrations associated with the maximum and minimum age limits of the till samples.

The ^{10}Be concentrations, corrected for radioactive decay, indicate that the two late Pliocene R2 till samples have the highest concentrations (1.35 and 1.87×10^{8} atoms/g), whereas the younger tills have concentrations that are an order of magnitude lower (3.72 to 5.99×10^{7} atoms/g; Table 2; Fig. 6). The ^{10}Be content of the R2 tills is, however, not as high as might be expected if they represent a source solely derived from a ^{10}Be-saturated saprolite mantle that had been exposed to meteoric precipitation for tens of millions of years. These lower concentrations could be related to several factors: loss of ^{10}Be through particulate erosion of the uppermost part of the regolith during preglacial times; erosion of the most ^{10}Be-enriched horizons by ice sheets during glaciations that preceded the that events led to the deposition of our older tills; and mixing of the uppermost horizon of the regolith with ^{10}Be-depleted sediments during glacial transport. Nevertheless, the R2 till concentrations are just slightly lower than the highest concentration reported from the uppermost part of an old saprolite (i.e., 1.46×10^{9} atoms/g [44]). Within the context of this study, the lower concentrations among the younger R1 and N tills suggest that the clayey and uppermost meters of the regolith enriched in ^{10}Be had been eroded by 1.3 Ma. Accordingly, the ^{10}Be content of tills supports the presence of a preglacial regolith and its subsequent erosion during late Pliocene and early Pleistocene glaciations.

7. Additional support for the hypothesis

Three marine tracers of continental weathering provide further support for the removal of a weathered rock mantle and exposure of fresh silicate bedrock during the MPT. The record of $^{87}Sr/^{86}Sr$ of dissolved Sr in seawater over the past 5 Ma is characterized by a nonlinear increase in $^{87}Sr/^{86}Sr$ ratios beginning ~2.7 Ma (Fig. 7). Although the general increase in seawater $^{87}Sr/^{86}Sr$ during the Cenozoic is often attributed to the uplift-induced weathering of ^{87}Sr-bearing lithologies in the Himalayan region, the mechanisms governing the major inflexions in the $^{87}Sr/^{86}Sr$ curve are still a subject of debate (e.g., [46]). For example, the onset of Northern Hemisphere glaciation may have contributed to the late Cenozoic rise in $^{87}Sr/^{86}Sr$ ratios through an increase in the flux of Sr from the continents and/or increase of the $^{87}Sr/^{86}Sr$ ratio of riverine Sr [42,47–50]. We further suggest that the two subsequent increases in the rate of change of $^{87}Sr/^{86}Sr$ that follow the initial inflection in $^{87}Sr/^{86}Sr$ ratios at ~2.7 Ma are related to the unroofing of the Canadian Shield by ice sheet erosion of the regolith and to the subsequent onset of 100-kyr glaciations. This argument is based on the fact that high $^{87}Sr/^{86}Sr$ ratios are found primarily in old sialic rocks (mainly in biotite) and that, conversely, old soils such as regolith are largely depleted in radiogenic Sr [42]. We thus attribute the initial increase in $^{87}Sr/^{86}Sr$ between ~2.7 and 1.4 Ma, at a rate of 0.033 ppm kyr^{-1}, to an increased flux of radiogenic Sr to the oceans derived from the onset of glacial activity in shield-rock regions (c.f. erosion of the regolith). Because subsequent exposure of fresh crystalline bedrock would expose silicate minerals to chemical weathering, we associate the accelerated rise in marine $^{87}Sr/^{86}Sr$ ratios starting at ~1.4 Ma (~0.1 ppm kyr^{-1}) to an increase in the $^{87}Sr/^{86}Sr$ ratios of river waters from the enhanced silicate weathering of newly exposed basement rocks, in addition to the enhanced Sr flux derived from continued glacial activity during high-frequency (41 kyr) glacial cycles. Finally, we attribute the decelerated rise in marine $^{87}Sr/^{86}Sr$ ratios after ~1 Ma (~0.037 ppm kyr^{-1}) to the onset of 100-kyr glaciation cycles, which would result in lower values of riverine $^{87}Sr/^{86}Sr$ ratios relative to those associated with 41-kyr cycles. The release of the most radiogenic Sr by weathering occurs during the initial stages of interglaciations, thus, the longer duration of interglacial weathering after the MPT would have resulted in the release of less radiogenic Sr, on average, in comparison with the shorter interglaciations associated with 41-kyr cycles [42,50].

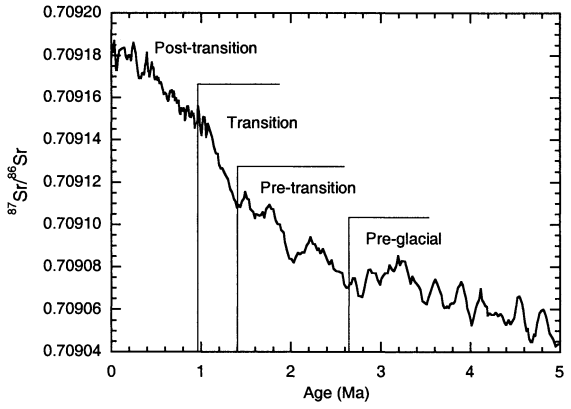

Fig. 7. Diagram showing changes in the marine $^{87}Sr/^{86}Sr$ isotope record for the past 5 Ma in the context of unroofing of fresh crystalline bedrock around the interval of the middle Pleistocene transition (data from [49], five-point running average). The boundaries for the MPT are arbitrary and were chosen according to the position of the main inflexions in the Sr record that are concomitant with changes in the amplitude and frequency of the $\delta^{18}O$ record.

A record of ε_{Hf} in seawater from NW Atlantic ferromanganese crusts also indicates changes associated with the onset of Northern Hemisphere glaciation. In this case, the overall decrease in ε_{Hf} values at ~2.5 Ma is attributed to an increase in glacial crushing of zircons, which are the primary reservoir of unradiogenic Hf [51]. Of significance here, however, is the fact that the decrease in ε_{Hf} values accelerated from ~2.5 Ma until sometime after ~1.7 Ma, at which point the rate of decrease remained constant to the present. We suggest that this trajectory of ε_{Hf} values may also reflect enhanced crushing of minerals in response to increasing surface area of exposed Canadian Shield rocks caused by progressive glacial erosion [8]. Exposure of hard bedrock at the ice-bed interface would induce greater mineral crushing relative to that associated with a soft, regolith-floored substrate [52]. Rates of mineral crushing would then remain constant when the entire shield became exposed, thus delivering a constant and high flux of unradiogenic Hf to the ocean.

Osmium is another tracer of continental weathering, with higher $^{187}Os/^{186}Os$ ratios indicating an increase in silicate weathering rates [53]. For example, the slightly more radiogenic nature of North Atlantic seawater compared with other ocean water masses may reflect the enhanced silicate weathering of recently deglaciated shield areas surrounding the North Atlantic Ocean [53]. Burton et al. [54] reported a constant $^{187}Os/^{186}Os$ ratio of seawater between 2.5 and 0.9 Ma, followed by a steep increase in the $^{187}Os/^{186}Os$ ratio to the present. Unlike Sr isotopes, the exchangeable fraction of radiogenic Os in highly weathered soils is strongly depleted relative to the bulk soil fraction that an increased continental flux of such material would not influence the $^{187}Os/^{186}Os$ ratio of seawater. Accordingly, Peucker-Ehrenbrink and Blum [53] suggested that the initial period of a constant $^{187}Os/^{186}Os$ ratio reflected regolith erosion by ice sheets, whereas subsequent exposure of unweathered shield bedrock ~0.9 Ma is reflected by an increase in the $^{187}Os/^{186}Os$ of seawater.

8. Discussion and conclusions

Because the MPT cannot be explained by orbital forcing [4,6], most explanations for the MPT invoke some forcing internal to the climate system. For instance, several ice sheet-climate models have simulated the MPT as a nonlinear response to a prescribed long-term cooling trend, possibly in response to a gradual decrease in atmospheric pCO_2 [55–57]. Other records, however, suggest that low pCO_2 has existed over the last 25 Myr [58,59], although the resolution and precision of these records may be too low to identify a decrease in pCO_2 that may induce a threshold from smaller to larger ice sheets with corresponding differences in response to orbital forcing [56]. Nevertheless, existing ice core records of pCO_2 [60] do not support the assumption of the continuation of a 3-Myr linear decrease in pCO_2 over the last 440 ka [55,56]. Forthcoming ice core records that extend over the last 1 Ma will shed important information on this issue.

Long-term cooling induced by other mechanisms would also provide a viable candidate for the MPT. For example, one model [57] simulates the MPT in response to late Cenozoic cooling of deep ocean water [5,61]. The relation between any such long-term cooling and the MPT remains unclear, however, particularly because the cooling may instead be a response to events associated with the MPT, such as increased ice sheet size [62]. According to this scenario, any cooling may then represent an important feedback on subsequent glacial dynamics but is not the primary forcing of the MPT.

Perhaps, the most important constraint that any mechanism for the MPT must address is the evidence that the gain in volume of post-transition ice sheets was accomplished through an increase in the thickness of already areally extensive ice sheets (Fig. 1; [8]). Models that simulate the MPT through long-term cooling do so as a consequence of an attendant increase in either ice volume [56] or sea ice extent [57], with a threshold occurring in both cases that triggers the onset of the 100-kyr glacial cycle. Although these models also simulate an increase in the amplitude of glacial cycles, they do not explicitly identify a mechanism that causes a transition from thin, areally extensive ice sheets to thick ice sheets of similar areal extent and thus do not satisfy this constraint imposed by the geologic record [19,25,63].

The regolith hypothesis provides such a mechanism. Ice-sheet thickness is controlled primarily by mechanisms at the base of the ice sheet that regulate ice motion. An ice sheet resting on soft, deformable sediments (such as regolith) moves by deformation of the underlying sediment, with some contribution from internal ice deformation and sliding at the ice/substrate interface. Accordingly, a soft-bedded ice sheet generally flows faster than does an ice sheet underlain by solid bedrock, where ice movement is limited due to the lack of subglacial sediment deformation [9–11]. As a result, a soft-bedded ice sheet will tend to be thinner than its hard-bedded counterpart (steeper surface slope). The regolith hypothesis proposes that the MPT occurred by progressive advection of the regolith through shear imposed by the overlying ice sheet, eventually exposing the hard bedrock to cause a change from thinner to thicker ice sheets with a corresponding difference in ice sheet response to orbital forcing (Fig. 1).

The regolith hypothesis makes a clear prediction that a fundamental change in the composition of

terrestrial and marine sediments should be concordant with the spectral change seen in the $\delta^{18}O$ record. Indeed, our results on the geochemistry, mineralogy, and petrology of midcontinent tills that span the MPT document the removal of an early bedrock source that was highly weathered, followed by a change to a source comprised of less weathered or fresh crystalline bedrock. Specifically, the oldest (R2) tills are depleted in crystalline lithologies and unstable minerals and are enriched in weathered products, as indicated by clay mineralogy and till geochemistry. In contrast, the younger tills show enrichment in crystalline lithologies and stable minerals and depletion in weathered products. High concentrations of meteoric ^{10}Be in R2 tills similarly indicate a regolith source for these old tills, whereas lower meteoric ^{10}Be concentrations in younger tills indicate that the upper clayey ^{10}Be-enriched horizon of the regolith had been eroded by ~1.3 Ma.

Changes in $^{87}Sr/^{86}Sr$ and $^{187}Os/^{186}Os$ ratios of seawater during the late Cenozoic further identify the removal of a highly weathered rock mantle and the subsequent unroofing of fresh, unweathered silicate rock around the onset of the MPT. Exposure of the hard-rock substrate at that time also increased physical crushing beneath the LIS, and the breakdown of weathering-resistant minerals like zircons may have led to increased flux of unradiogenic Hf to the ocean. We note that weathering of newly exposed silicate bedrock during the MPT may have provided an important sink of CO_2 [42], with attendant cooling perhaps representing an important feedback to the onset and maintenance of the 100-kyr cycles.

In summary, the MPT is characterized by a change from low-amplitude, high-frequency glacial cycles to high-amplitude, low-frequency glacial cycles in the absence of any change in orbital forcing. Records of global ice volume and ice sheet extent indicate that, while the volume of ice sheets increased significantly after the MPT, the areal extent of ice sheets remained largely the same. The regolith hypothesis accommodates these changes by providing an explicit mechanism to cause a transition from thin to thick ice sheets [8]. Fundamental changes in the petrography and geochemistry of midcontinent tills and the geochemistry of seawater during the MPT are consistent with the prediction of unroofing of Precambrian Shield bedrock by ice sheet erosion of regolith. We thus conclude that regolith erosion and the attendant change in the basal boundary conditions of the LIS best explain the geologic constraints (records of ice extent and ice volume) associated with the MPT.

Acknowledgements

J. Stone and G. Balco are thanked for useful suggestions on the ^{10}Be extraction method. Suzanne Anderson, David Bowen, and one anonymous reviewer provided helpful and constructive comments on the manuscript. The National Science Foundation (ATM 9709684) supported this study.

Appendix A. Supplementary data

Supplementary data associated with this article can be found, in the online version, at doi:10.1016/j.epsl.2004.09.001.

References

[1] J.D. Hays, J. Imbrie, N.J. Shackleton, Variations in the Earth's orbit: pacemaker of the ice ages, Science 194 (1976) 1121–1132.
[2] J. Imbrie, J.D. Hays, D.G. Martinson, A. MacIntyre, A.C. Mix, J.J. Morley, N.G. Pisias, W. Prell, N.J. Shackleton, The orbital theory of Pleistocene climate: support for a revised chronology of marine d^{18}O record, in: A.L. Berger, J. Hays, G. Kukla, B. Salzman (Eds.), Milankovitch and Climate: Part 1, Dordrecht Reidel, Norwell, 1984, pp. 269–305.
[3] A.C. Mix, N.G. Pisias, W. Rugh, J. Wilson, A. Morey, T.K. Hagelberg, Benthic foraminifer stable isotope record from site 849 (0–5 Ma): local and global climate changes, Proc. Ocean Drill. Prog., Sci. Results 138 (1995) 342–371.
[4] N.G. Pisias, T.C. Moore Jr., The evolution of the Pleistocene climate: a time series approach, Earth Planet. Sci. Lett. 52 (1981) 450–458.
[5] W.F. Ruddiman, M.E. Raymo, D.G. Martinson, B.M. Clement, J. Backman, Pleistocene evolution: Northern Hemisphere ice sheets and North Atlantic Ocean, Paleoceanography 4 (1989) 353–412.
[6] J. Imbrie, et al., On the structure and origin of major glaciations cycles: 2. The 100,000-year cycle, Paleoceanography 8 (1993) 699–735.
[7] M. Elkibbi, J.A. Rial, An outsider's review of the astronomical theory of the climate: is the eccentricity-driven insulation the main driver of the ice ages? Earth-Sci. Rev. 56 (2001) 161–177.

[8] P.U. Clark, D. Pollard, Origin of the middle Pleistocene transition by ice sheet erosion of regolith, Paleoceanography 13 (1998) 1–19.
[9] G.S. Boulton, A.S. Jones, Stability of temperate ice caps and ice sheets resting on beds of deformable sediments, J. Glaciol. 24 (1979) 29–43.
[10] R.B. Alley, D.D. Blankenship, C.R. Bentley, S.T. Rooney, Deformation of till beneath ice stream: B. West Antarctica, Nature 322 (1986) 57–59.
[11] P.U. Clark, R.B. Alley, D. Pollard, Northern Hemisphere ice sheet influences on global climate change, Science 286 (1999) 1104–1111.
[12] S.S. Goldich, A study in rock weathering, J. Geol. 46 (1938) 17–58.
[13] H.W. Nesbitt, G.M. Young, Formation and diagenesis of weathering profiles, J. Geol. 97 (1989) 129–147.
[14] D.R. Setterholm, G.B. Morey, An extensive pre-Cretaceous weathering profile in east-central and southwestern Minnesota, U.S. Geol. Surv. Bull. 1989 (1995) (29 pp.).
[15] G.R. Hallberg, Pre-Wisconsinan glacial stratigraphy of the central plains region in Iowa, Nebraska, Kansas, and Missouri, Quat. Sci. Rev. 5 (1986) 11–15.
[16] G.A. Izett, Volcanic ash beds: recorders of upper Cenozoic silicic pyroclastic volcanism in the western United States, J. Geophys. Res. 86 (1981) 10200–10222.
[17] C.A. Gansecki, G.A. Mahood, M. McWilliams, New ages for the climatic eruptions at Yellowstone: single-crystal $^{40}Ar/^{39}Ar$ dating identifies contamination, Geology 26 (1998) 343–346.
[18] J. Boellstorff, North American Pleistocene stages reconsidered in the light of probable Pliocene–Pleistocene continental glaciation, Science 202 (1978) 305–307.
[19] M. Roy, P.U. Clark, R.W. Barendregt, J.R. Glasmann, R.J. Enkin, Glacial stratigraphy and paleomagnetism of late Cenozoic deposits in the north-central United States, Geol. Soc. Amer. Bull. 116 (2004) 30–41.
[20] P.R. Bierman, K.A. Marsella, C. Patterson, P.T. Davis, M. Caffee, Mid-Pleistocene cosmogenic minimum-age limits for pre-Wisconsinan glacial surfaces in southwestern Minnesota and southern Baffin Island: a multiple nuclide approach, Geomorphology 27 (1999) 25–39.
[21] J.S. Aber, Pre-Illinoian glacial geomorphology and dynamics in the central United States, west of the Mississippi, in: D.M. Mickelson, J.W. Attig (Eds.), Glacial Processes Past and Present: Boulder, Colorado, Special Paper-Geol. Soc. Am., vol. 327, 1999, pp. 113–119.
[22] A.S. Dyke, V.K. Prest, Late Wisconsinan and Holocene history of the Laurentide ice sheet, Géogr. Phys. Quat. 41 (1987) 237–263.
[23] M. Roy, P.U. Clark, R.A. Duncan, S.R. Hemming, Constraints on Laurentide ice sheet ice flow geometry from $^{40}Ar/^{39}Ar$ provenance studies of glacial deposits, EOS Trans., AGU 85 (17) (2004) (Jt. Assem. Suppl., Abstract C43A-22).
[24] J. Boellstorff, Tephrochronology, petrology, and stratigraphy of some Pleistocene deposits in the Central Plains, USA, PhD thesis, Louisiana State University, Baton Rouge, 197 pp.
[25] J. Boellstorff, Chronology of some Late Cenozoic deposits from the central United States and the ice ages, Trans. Nebr. Acad. Sci. 6 (1978) 35–49.
[26] D.M. Shaw, G.A. Reilly, J.R. Muysson, G.E. Pattenden, F.E. Campbell, An estimate of the composition of the Canadian Precambrian Shield, Can. J. Earth Sci. 4 (1967) 829–853.
[27] D.M. Shaw, J. Dostal, R.R. Keys, Additional estimates of continental surface Precambrian shield composition in Canada, Geochim. Cosmochim. Acta 40 (1976) 73–84.
[28] R.S. Taylor, S.M. McLennan, The Continental Crust: Its Composition and Evolution, Blackwell, Oxford, 1985, 312 pp.
[29] K.H. Wedepohl, The composition of the continental crust, Geochim. Cosmochim. Acta 59 (1995) 1217–1232.
[30] H.W. Nesbitt, G. Markovics, Weathering of granodiorite crust, long-term storage of elements in weathering profiles, and petrogenesis of siliciclastic sediments, Geochim. Cosmochim. Acta 61 (1997) 1653–1670.
[31] G. Taylor, R.A. Eggleton, Regolith Geology and Geomorphology, John Wiley & Sons, 2001, 375 pp.
[32] C. Ollier, C. Pain, Regolith, Soil and Landforms, John Wiley & Sons, Chichester, NY, 1996, 309 pp.
[33] W.E. Parham, Clay mineralogy and geology of Minnesota kaolin's clay, Spec. Publ. Ser.-Minn. Geol. Surv. SP-10 (1970) (142 pp.).
[34] M. Bouchard, S. Jolicoeur, Chemical weathering studies in relation to geomorphological research in southeastern Canada, Geomorphology 32 (2000) 213–238.
[35] C.P. Gravenor, Erosion by continental ice sheets, Am. J. Sci. 275 (1975) 594–604.
[36] F. Thiebault, M. Cremer, P. Bebrabant, J. Foulon, O.B. Nielson, H. Zimmerman, Analysis of sedimentary facies, clay mineralogy, and geochemistry of the Neogene–Quaternary sediments in site 645, Baffin Bay, Proc. Ocean Drill. Prog., Sci. Results 105 (1989) 83–100.
[37] J.T. Andrews, Changes in the silt- and clay-size mineralogy of sediments at Ocean Drilling Program site 645B, Baffin Bay, Can. J. Earth Sci. 30 (1993) 2448–2452.
[38] G. Faure, Principles and Applications of Geochemistry, 2nd ed., Prentice-Hall, New Jersey, 1998, 600 pp.
[39] H.W. Nesbitt, G.M. Young, Early Proterozoic climates and plate motions inferred from major element chemistry, Nature 299 (1982) 715–717.
[40] A.S. Dyke, J.T. Andrews, P.U. Clark, J.H. England, G.H. Miller, J. Shaw, J.J. Veillette, The Laurentide and Innuitian ice sheets during the last glacial maximum, Quat. Sci. Rev. 21 (2002) 9–31.
[41] A. Taylor, J.D. Blum, Relation between soil age and silicate weathering rates determined from the chemical evolution of a glacial chronosequence, Geology 23 (1995) 979–982.
[42] J.D. Blum, The effect of late Cenozoic glaciation and tectonic uplift on silicate weathering rates and the marine $^{87}Sr/^{86}Sr$ record, in: W.F. Ruddiman (Ed.), Tectonic Uplift and Climate Change, Plenum Press, New York, 1997, pp. 259–288.
[43] M.J. Pavich, L. Brown, J. Klein, R. Middleton, Beryllium-10 accumulation in a soil chronosequence, Earth Planet. Sci. Lett. 68 (1984) 198–204.

[44] M.J. Pavich, L. Brown, N.J. Valette-Silver, J. Klein, R. Middleton, ^{10}Be analysis of a quaternary weathering profile in the Virginia Piedmont, Geology 13 (1985) 39–41.
[45] J.O. Stone, A rapid fusion method for separation of beryllium-10 from soils and silicates, Geochim. Cosmochim. Acta 62 (1998) 555–561.
[46] W.F. Ruddiman, Tectonic Uplift and Climate Change, Plenum Press, New York, 1997, 535 pp.
[47] R.L. Armstrong, Glacial erosion and the variable isotopic composition of strontium in seawater, Nature 230 (1971) 132–133.
[48] R.C. Capo, D.J. DePaolo, Seawater strontium isotopic variations from 2.5 million years ago to present, Science 249 (1990) 51–55.
[49] J.W. Farrel, S.C. Clemens, L.P. Gromet, Improved chronostratigraphic reference curve of late Neogene seawater ^{87}Sr/^{86}Sr, Geology 23 (1995) 403–406.
[50] J.D. Blum, Y. Erel, A silicate weathering mechanism linking increase in marine ^{87}Sr/^{86}Sr with global glaciation, Nature 373 (1995) 415–418.
[51] T. van der Flierdt, M. Frank, D. Lee, A.N. Halliday, Glacial weathering and the hafnium isotope of seawater, Earth Planet. Sci. Lett. 198 (2002) 167–175.
[52] K.M. Cuffey, R.B. Alley, Is erosion by deforming subglacial sediments significant? (towards till continuity), Ann. Glaciol. 22 (1996) 17–24.
[53] B. Peucker-Ehrenbrink, J.D. Blum, Re–Os isotope systematics and weathering of Precambrian crustal rocks: implications for the marine osmium isotope record, Geochim. Cosmochim. Acta 62 (1998) 3193–3203.
[54] K.W. Burton, J.L. Birck, C.J. Allegre, R.K. O'Nions, Fine scale records of seawater ^{187}Os/^{186}Os, Eos 76 (1995) 182.
[55] M.E. Raymo, Glacial puzzles, Science 281 (1998) 1467–1468.
[56] A. Berger, X.S. Li, M.F. Loutre, Modeling northern hemisphere ice volume over the last 3 Ma, Quat. Sci. Rev. 18 (1999) 1–11.
[57] E. Tziperman, H. Gildor, On the mid-Pleistocene transition to 100-kyr glacial cycles and the asymmetry between glaciation and deglaciation times, Paleoceanography 18 (2003).
[58] M. Pagani, M.A. Arthur, K.H. Freeman, Miocene evolution of atmospheric carbon dioxide, Paleoceanography 14 (1999) 273–292.
[59] P.N. Pearson, M.R. Palmer, Estimating Paleogene atmospheric pCO_2 using boron isotope analysis of Foraminifera, in: B. Schmitz, B. Sundquist, F.P. Andreasson (Eds.), Early Paleogene Warm Climates and Biosphere Dynamics, Short Papers and Extended Abstracts, vol. 122, Geological Society of Sweden, Stockholm, Sweden, 2000, pp. 127–128.
[60] J.R. Petit, et al., Climate and atmospheric history of the past 420,000 years from the Vostok ice core, Antarctica, Nature 399 (1999) 429–436.
[61] K. McIntyre, A.C. Ravelo, M.L. Delaney, North Atlantic intermediate waters in the late Pliocene to early Pleistocene, Paleoceanography 14 (1999) 324–335.
[62] M. Ghil, S. Childress, Topics in geophysical fluid dynamics, atmospheric dynamics, dynamo theory, and climate dynamics, in: Applied Mathematical Sciences, vol. 60, Springer, New York, 1987, 485 pp.
[63] J.E. Joyce, L.R.C. Tjalsma, J.M. Prutzman, North American glacial meltwater history for the past 2.3 My, oxygen isotope evidence from the Gulf of Mexico, Geology 21 (1993) 483–486.